Microscopic calculations of medium effects for 200-MeV $(\vec{p},\vec{p}')$ reactions

F. Sammarruca
University of Idaho, Moscow, Idaho 83843

E. J. Stephenson and K. Jiang*
Indiana University Cyclotron Facility, Bloomington, Indiana 47408

(Received 22 December 1998; revised manuscript received 3 June 1999; published 15 November 1999)

We present a *G*-matrix calculation of the effective nucleon-nucleon (*NN*) interaction for the distorted wave impulse approximation prediction of the cross section and polarization observables in (p,p') reactions. This interaction is based on a one-boson-exchange model of the free *NN* force that reproduces *NN* observables well. The *G* matrix includes the effects of Pauli blocking, nuclear binding, and strong relativistic mean-field potentials. To assess the quality of this interaction, we compare to 200-MeV measurements of the cross section and analyzing power for natural-parity inelastic transitions in ^{16}O, ^{28}Si, and ^{40}Ca that span a variety of spins and nuclear densities, as well as to the interaction developed by Furnstahl and Wallace within a relativistic framework. [S0556-2813(99)02912-X]

PACS number(s): 25.40.Ep, 21.30.Fe, 24.10.Cn, 24.70.+s

I. INTRODUCTION

One of the goals of nuclear physics is to describe the structure of nuclei and the dynamics of nuclear reactions in terms of the underlying interaction between nucleons. But from a practical standpoint a microscopic calculation of the many-body system is not a viable option. One simplification of the nuclear many-body problem is the construction of an effective nucleon-nucleon (*NN*) interaction, modified so as to account for the presence of the many-body environment, that can be used in a treatment of the properties of nuclear matter or nuclear reactions.

The most commonly included many-body mechanisms arise from Pauli blocking and nuclear binding, and are the main aspects of what is known as the Brueckner *G*-matrix approach (BHF) [1–6]. Effective interactions of this type have been used as the basis for many calculations of proton elastic and inelastic scattering [7–21], in some cases with considerable success. However, the same approach fails to predict correctly the saturation properties of nuclear matter [22]. More successful in that regard is the relativistic extension of the Brueckner theory [23–26], which has also become an established method for nuclear matter studies. Known as Dirac-Brueckner theory (DBHF), the method characterizes the nuclear mean field by strong, competing vector and scalar fields that together account for both the binding of nucleons and the large size of the spin-orbit splitting seen in nuclear states. Effective interactions that include these relativistic effects have seen much less application to the study of proton-induced reactions [27–29], and in fact have been compared only to natural-parity inelastic transitions. We will refer here to all of these effects as ''conventional'' medium modifications.

Measurements of the polarization observables for proton-induced quasielastic scattering [30–33] and the excitation of unnatural-parity states [34–37] have been more difficult to describe. BHF approaches are generally not adequate [33,38]. The inclusion of relativistic effects is helpful in the quasielastic case [39,40]. The problems encountered with polarization observables have been associated with the existence of more exotic medium effects. Among those, one of the most extensively discussed is the possible reduction of meson masses as a consequence of changes to the QCD vacuum in the nuclear medium [41–43]. In future papers we intend to investigate these issues. Starting from effective interactions based on DBHF methods, we will confront a variety of unnatural-parity (p,p') transitions and explore issues such as meson mass scaling.

In this paper, our primary purpose is to present the DBHF technique we will use, and assess its quality in comparisons to elastic and natural-parity inelastic transitions. For these data, the medium effects in both BHF and DBHF density-dependent interactions are large. The opportunity exists to see how well the medium-modified interaction follows data for transitions that vary in average nuclear density, and in spin and momentum transfer. As a part of this evaluation, we will examine our approach in comparison to the relativistic treatment of Furnstahl and Wallace. We will raise and test various distorted-wave impulse approximation (DWIA) model issues, including the treatment of the exchange amplitudes and optical model distortions. Taken together, these tests will reveal the systematic features of the effective interaction and help to gauge its reliability within DWIA so that its strengths and limitations are understood. This information should prove essential in extending the present ideas and methods in future work.

We describe in Sec. II the main ingredients of our model, starting with a one-boson-exchange (OBE) representation of the nucleon-nucleon (*NN*) interaction that provides an excellent reproduction of the *NN* observables below pion production threshold. This is an improved version of the Bonn-*B* potential [22]. The density-dependent effective interaction is obtained by solving the Bethe-Goldstone equation in infinite nuclear matter. It contains all the conventional effects as defined above, and correctly reproduces the saturation proper-

*Present address: MCI WorldCom, Oakbrook Terrace, IL 60181.

ties of nuclear matter. Next the resulting G matrix is converted to a Yukawa-function representation [44] for use in DWIA calculations, for which we employ the LEA program from Kelly [45].

Relativistic calculations for the case of inelastic scattering are relatively few. Here we will compare our results with the work of Furnstahl and Wallace [27,28], where the nucleons in the nucleus are described by Dirac bound states. These authors consider specific finite nuclei, and point out that the density-dependent effects for the elastic-scattering channel are less than those for the reaction channels because of the identity between initial and final states in the elastic case. In our work, the G matrix is constructed for infinite nuclear matter, and no such distinction exists. In particular, apart from the Cheon effect to be discussed in Sec. II C, we use the same effective interaction for elastic and inelastic scattering. The implications of this difference in approach will be examined in Sec. III.

Since the primary purpose of this paper is to evaluate our treatment of conventional medium effects, in Sec. III we will compare our predictions to measurements of the cross section and analyzing power for several natural-parity, isoscalar (p,p') transitions. We have chosen the data of Seifert [46] on ^{16}O and ^{40}Ca (200 MeV) and Chen [47] on ^{28}Si (180 MeV) since these are the same energies and targets that will appear in a future consideration of exotic medium effects for polarization transfer measurements. For natural parity transitions, polarization transfer measurements do not add new information to the analysis beyond that contained in the cross section and analyzing power [48] and will not be considered here.

II. THE MODEL

A. The nucleon-nucleon interaction

The starting point for a microscopic calculation of (p,p') reactions is a realistic free-space *NN* interaction which reproduces well *NN* scattering observables. Below the pion production threshold, we would expect that a one-boson-exchange basis would prove adequate. This is a quantitative reduction of a more comprehensive model containing multiple meson-exchange diagrams [22].

In this work, we will use an improved version of the Bonn-*B* potential [22]. We have chosen pseudovector coupling for the pion, and solve for the *NN* interaction through the use of the Thompson equation [49]. The major bosons in the model are (a) the pseudoscalar pion, which is the lightest and hence longest ranged of the mesons and which provides most of the attractive tensor force, (b) the ρ vector meson, a two-pion P-wave resonance that provides a short-range repulsive tensor force, (c) the ω vector meson, a three-pion resonance that creates a strong, repulsive central force at short range and that contributes to the spin-orbit force, and (d) the fictitious isoscalar-scalar σ meson that represents two-pion S-wave exchange and that contributes to the medium range attraction necessary to bind the nucleus. The OBE amplitudes for these mesons are given explicitly in Refs. [22,50]. Since the parameters of the original Bonn-*B* interaction were determined about a decade ago, there has been substantial progress in both high-precision measurements of *NN* scattering and phase-shift analyses. Since a good fit to the *NN* data is a crucial prerequisite for an evaluation of the quality of the (p,p') calculations, the parameters of the model have been adjusted to bring the predictions into better accord with current phase shift analyses from the Nijmegem group up to 325 MeV [51]. The σ meson is now different in the two isospin channels. As a consequence of this extra degree of freedom, the δ meson becomes unimportant and is, therefore, omitted. The values for the masses, coupling constants, and cutoff parameters for the mesons are given in Table I. This scheme alone is not fully satisfactory in the $T=1$ channel. So in a manner similar to that used in the construction of the (charge-dependent) CD-Bonn interaction [52], adjustments have been made to the σ-meson coupling constant for some individual partial waves. These altered values are given in Table II. A comparison with *NN* data measured near 200 MeV was found to be excellent.

TABLE I. OBE meson properties.

Meson	Mass (MeV)	Coupling $(g^2/4\pi)$	Cutoff (MeV)
π	138.03	13.8	1700
η	548.8	3	1500
ρ	769	0.99 $(f_\rho/g_\rho=6.1)$	1300
ω	782.6	2	1500
σ $(T=0)$	550	5.966	2000
σ $(T=1)$	550	8.5	2000

The importance of using an accurate *NN* interaction becomes apparent in Fig. 1, where we show calculations for the ^{40}Ca$(p,p')^{40}$Ca reaction to the 3^- state at 3.736 MeV based on this work and several other interactions. The techniques behind these calculations will be described more fully in Sec. II C. Here we concentrate only on the sensitivity of typical inelastic-scattering observables to the underlying *NN* force. For simplicity, none of the calculations shown in this test contain density dependence; i.e., they correspond to free-space *NN* forces. The top panels of Fig. 1 show predictions from our work (solid) and three modern high-precision potentials, specifically CD-Bonn [52] (long dash), NIJMEGEN-II [51] (medium dash), and REID93 [51] (short dash). The lower panel shows five predictions based upon older interactions, including Franey and Love [53] (solid), Bonn-*B* [19] (long dash), Paris [54] (medium dash), von Geramb [15] (short dash), and Reid [55] (long and short dash), which are not as accurate in describing the most modern *NN* data. Clearly, the various curves are much more scattered in the lower panel, implying considerably larger theoretical uncertainty. On the

TABLE II. σ meson couplings.

Partial wave	Coupling $(g^2/4\pi)$
$^3P_1$	8.9
$^1D_2$	10.05
$^3P_2$	9.11
$^3F_3$	13.5

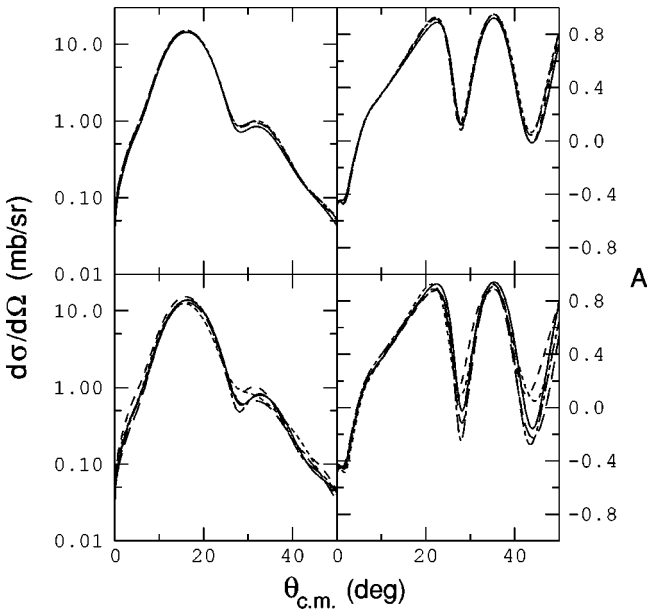

FIG. 1. A comparison of free interaction calculations for the ^{40}Ca$(p,p')^{40}$Ca reaction to the 3^- state at 3.736 MeV. The upper panels compare our interaction (solid) with CD-Bonn [52] (long dash), NIJMEGEN-II [51] (medium dash), and REID93 [51] (short dash). The lower panel contains the older interactions of Franey and Love [53] (solid), Nakayama and Love based on the older Bonn-B [19] (long dash), Paris [54] (medium dash), von Geramb and Rikus [15] (short dash), and Reid [55] (long and short dash).

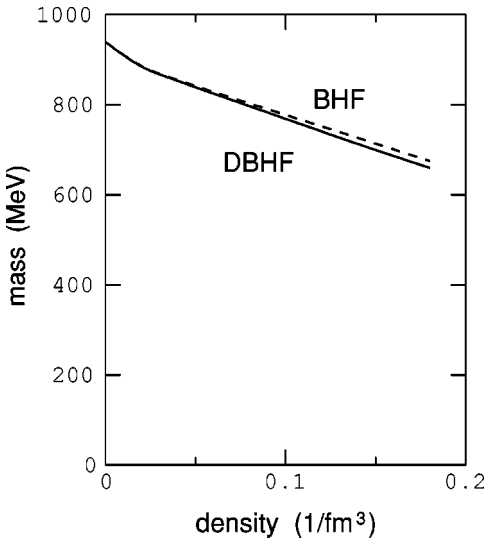

FIG. 2. The effective nucleon mass as a function of the Fermi momentum k_F corresponding to the BHF (dashed) and DBHF (solid) calculations, respectively.

scale of our comparison to (p,p') data such differences do matter. A similar conclusion is illustrated for unnatural-parity transitions by Fig. 2 of Ref. [56]. In general, older interactions are not as faithful to present *NN* scattering data, and are likely to show larger discrepancies when compared to (p,p') data. Thus it is important to start from an accurate two-body input.

Our full density-dependent interaction is constructed within the DBHF approach to infinite nuclear matter. However, for purposes of illustration, we will also present predictions obtained within the BHF framework, where medium effects come in through a (spherically averaged) Pauli operator and modification of the single-particle energy in nuclear matter.

In the DBHF scheme, the mean nuclear potential is expressed in terms of an attractive scalar and a repulsive vector field. This approach was initiated in the 1970s by Clark and collaborators [57] and applied to proton-nucleus elastic scattering with significant improvement to the spin observables. Here we follow closely the relativistic approach to nuclear matter as reviewed in Chap. 10 of Ref. [22]. The modifications to the nucleon Dirac spinor arising from such strong fields produce a characteristic repulsive effect that is crucial to describe correctly the saturation properties of nuclear matter. This repulsion appears also in the real central isoscalar effective interaction. There the effects of the BHF and DBHF density dependence are similar in kind, but typically much larger in the DBHF case.

As explained in detail in Ref. [5], the calculation of the *G* matrix (for both BHF and DBHF) poses a self-consistency problem, since the *G* matrix and the (unknown) nuclear matter potential are related to each other. The numerical procedure is facilitated by the so-called effective mass ansatz, in which the single-particle energy is approximated by a suitable analytic function (see Sec. 3.2 of Ref. [5], or Sec. 10.5 of Ref. [22] for the relativistic treatment). In choosing the function, we reproduce momenta above the Fermi level, in contrast to other calculations [22], because this improves the quality of the approximation near the beam momentum. The resulting nucleon effective masses, shown in Fig. 2, are larger (namely, closer to their free-space value) and yield weaker density-dependent effects than do those interactions which do not reproduce the single-particle potential above the Fermi momentum. The self-consistent calculation that produces the effective masses used here saturates nuclear matter (in the DBHF case) at the realistic value of 0.17 nucleons/fm^3 with a binding energy of 14.4 MeV.

B. Transformation to an effective *NN* interaction

If the *t*- or *G*-matrix interaction is to be useful in existing distorted-wave impulse approximation (DWIA) calculations, the *NN* amplitudes must be expanded in a series of coordinate-space functions. The usual choice is a set of Yukawa functions, since these resemble some of the shapes involved in the OBE potential. A parametrization using such functions by Love and Franey [44] requires very few terms, so we have adopted their choice of Yukawa functions and ranges as our basis.

The transformation between partial wave matrix elements and the coefficients of a Yukawa expansion are described in Appendix A. There the one-step fitting process is also detailed. The quality of this transformation has been checked by inversion, and the reproduction of the original matrix elements is excellent. In addition, the same Yukawa coefficients can be used to expand the interaction in momentum space. When a free interaction is expanded this way, the resulting amplitudes can be used to calculate *NN* scattering

angular distributions that compare well with *NN* cross section and polarization measurements.

C. The DWIA calculations

In this subsection, we describe the main features of the DWIA calculations that will be compared in Sec. III with the cross section and analyzing power for a number of natural-parity (p,p') transitions. This involves several choices concerning which DWIA program to use, and how to treat the distortions and structure as well as the interaction. Some of these choices can be tested, and the results of such tests will be discussed at the beginning of Sec. III.

In the original work where these (p,p') data were reported [46,47], measurements of the cross section and analyzing power were matched with a phenomenological effective *NN* interaction using the DWIA program LEA [45]. We have used this program here since it incorporates a number of desirable features. For later studies of unnatural-parity transitions, the treatment of exchange will become a more serious problem that requires the use of a finite-range program for the exchange part of the scattering.

LEA makes use of a pseudopotential form of the Born approximation in which each term of the effective *NN* interaction is folded with the appropriate piece (depending on spin operator coupling) of the nuclear density. The resulting effective potential is then used to calculate the transition amplitude by overlapping it with a distorted-wave description of the projectile motion and the appropriate piece of the transition density. In this scheme medium effects are determined at a density evaluated at the spatial coordinate of the projectile. Thus it is most appropriate for the calculation of the direct part of the scattering. Exchange is handled in a zero-range approximation that adds this piece of the effective *NN* interaction to the direct part, and the overlap is calculated as it would be if the outgoing nucleon were the projectile. Unlike prior applications of LEA, the kinematics for the exchange amplitude added here use a momentum transfer calculated by assuming that the struck nucleon is in motion prior to the collision with a momentum that has the smallest possible value in the target frame of reference (see Appendix B). For large target masses, this choice converges to the Breit frame.

The entrance and exit channel distortions are calculated using a first-order folding prescription $(t\rho)$. The same density-dependent interaction is used for both the elastic and inelastic calculations except for the small change to the exchange part required by the different reaction Q value (Appendix B). However, there are corrections to the density dependence that are different between the elastic and the inelastic channels [58,59], and these have been included. In addition, we incorporate a small downward rescaling of the effective *NN* interaction resulting from transforming the *NN* interaction from the nucleon-nucleon to the nucleon-nucleus frame of Refs. [44,60].

The ground-state nuclear matter density is needed to determine the density at which the interaction should be evaluated. We have taken the longitudinal form factor for elastic electron scattering [61] from each target and corrected it for the charge distribution of the proton using an unfolding procedure available in LEA. What remains from the deconvolution is assumed to be a point nucleon density that applies to both protons and neutrons, since all of the targets considered here have equal proton and neutron numbers. This density is then evaluated at the position of the projectile.

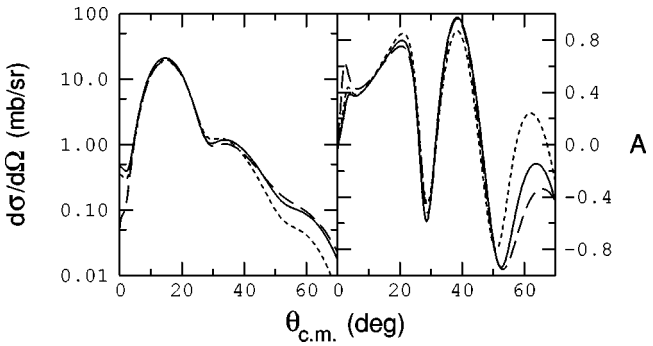

FIG. 3. Calculations of the cross section and analyzing power for the first 2^+ state in ^{28}Si. The short-dash curves use the structure form factor of Chen [47]. The solid and long dashed curves use shell-model transitions densities. The solid calculations are made with LEA, while the long-dash curves use the program DWBA86.

The transition form factors have been calculated by Seifert [46] and Chen [47] in a series expansion based again on longitudinal electron-scattering measurements. We use their expansions here. The accurate representation of the form factor is one of the important advantages of using LEA. Thus this uncertainty is removed in the comparison with (p,p') data.

III. DWIA RESULTS AND DISCUSSION

A. Verification of the model

Before comparing our calculations to a broad range of (p,p') transitions, we will examine a number of issues relating to the model described in Sec. II. Elastic and inelastic data will be used for comparisons. One such issue relating to the quality of the *NN* model was examined in Fig. 1.

If the strength of using LEA is the quality of the transition density, its weakness is the use of a zero-range exchange integral. This approximation can be checked by comparing to DWBA86 [62,63], one of a series of finite-range DWIA programs based on the work of Schaeffer and Raynal, provided the inputs can be made identical. When using DWBA86, transitions must be described as a series of particle-hole amplitudes. We obtained the particle-hole amplitudes for the first 2^+ state in ^{28}Si from the shell-model program OXBASH [64] running the *sd*-shell interaction of Wildenthal [65]. Using harmonic-oscillator wave functions ($b=1.808$ fm) and scaling all amplitudes up to account for collectivity, the cross sections and analyzing powers (see Fig. 3) from LEA (solid) and DWBA86 (long dashed) are essentially identical. The LEA result using the best-fit transition density (short dash) differs more noticeably. Thus it is important to avoid shell-model expansions unconstrained by electron scattering, and we lose no precision for natural-parity transitions with the zero-range calculations of LEA.

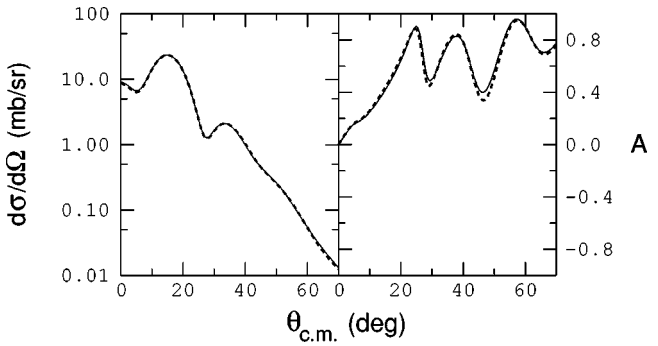

FIG. 4. Calculations of the cross section and analyzing power for the first 2^+ state in ^{28}Si. The thin solid curves use the original zero range approximation of LEA [45], while the dashed curves use the formulation described in Appendix B. The interaction is the free *t* matrix described in Sec. II.

Figure 4 shows a similar check for the treatment of the kinematics of exchange as described in Sec. II C and Appendix B. The solid curve uses the older LEA treatment in which the exchange momentum transfer is a constant. Our prescription, shown by the dashed line, is nearly the same.

There have been two kinds of distortions used in DWIA calculations. Best-fit optical model calculations use potentials adjusted to reproduce proton elastic-scattering data on the same target and at the same bombarding energy as the inelastic measurements. Another prescription for the distorting potential is the folding model that convolves the isoscalar central and spin-orbit interactions with the point nucleon density. Although we will use the folding model in our applications, a comparison between these two models is illustrated in Fig. 5. The top panels show the best-fit (dashed) and folded (solid) elastic-scattering calculations in comparison to the measurements for ^{28}Si at 180 MeV [66]. The adjustment of the best-fit potential to the data succeeds in describing almost all of the points. The folding of the DBHF interaction yields a cross section calculation that becomes too large as the scattering angle increases and overly negative predictions for the analyzing power. In the lower panels these two distortion models are used in DWIA calculations using the DBHF density-dependent interaction for the (p,p') reaction to the first excited 2^+ state of ^{28}Si. In both cases the cross section is too large. The crucial difference is for the analyzing power, where the measurements are much better described by the folding model distortions. The folding model optical potential has a repulsive inner core that is absent from the best-fit potential. While such a core is needed at 200 MeV to understand scattering from lighter targets such as ^{12}C [67], it is not required in phenomenological optical model potentials for targets in the mass range of interest here [68].

More insight into the difficulties we encounter with the description of elastic scattering using the DBHF model can be obtained by a comparison of this model to similar work by Furnstahl and Wallace [27], based on the relativistic *NN* model of Ref. [69]. By solving the Dirac equation in a finite nuclear system, Furnstahl and Wallace produce effective interactions for specific nuclei. Their effective interactions suitable for the elastic or the inelastic case are different,

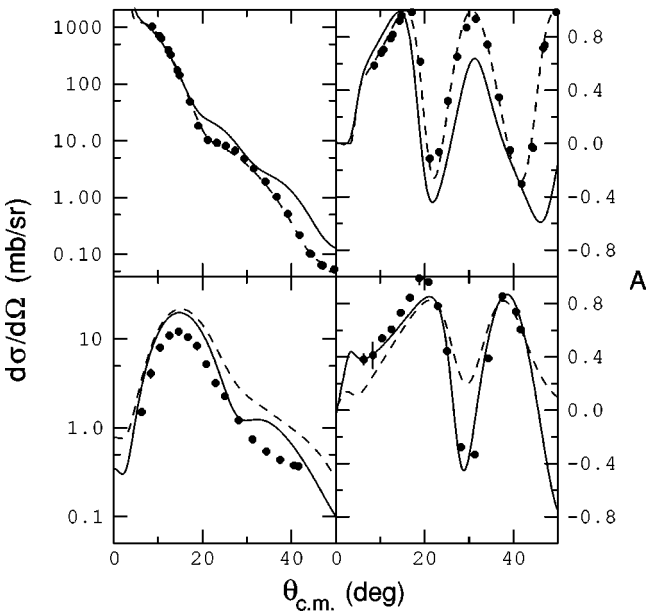

FIG. 5. Measurements of the cross section and analyzing power for elastic proton scattering from ^{28}Si at 180 MeV (top panels) and for inelastic proton scattering to the first 2^+ state in ^{28}Si (bottom panels). The elastic and inelastic-scattering calculations make use of best-fit optical potentials (dashed) or folding model potentials (solid).

since in the elastic case the identity between entrance and exit channels removes one power of the Möller operator from the scattering amplitude [27], which reduces relativistic medium effects. In Fig. 6, the top panels show our DBHF

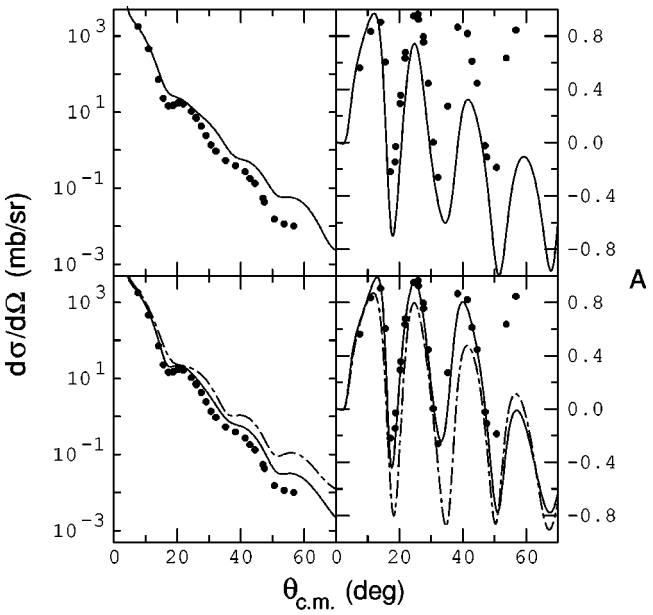

FIG. 6. Measurements of the cross section and analyzing power for proton elastic scattering from ^{40}Ca at 200 MeV. The folding model calculations were made using our DBHF interaction (top panels) or the elastic (solid curves, lower panels) and inelastic (long and short dash curves, lower panels) interactions of Furnstahl and Wallace.

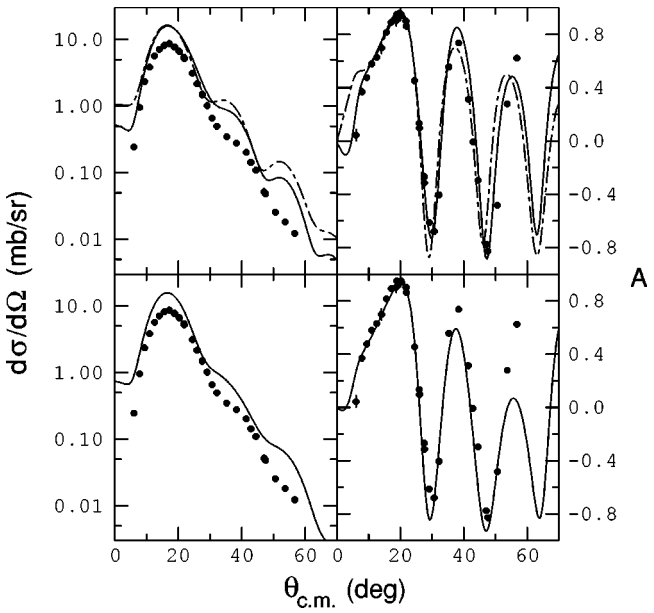

FIG. 7. Measurements of the cross section and analyzing power for the first 3^- state in ^{40}Ca. The upper panel curves are DWIA calculations using folding model distortions based on the elastic (solid) and inelastic (long and short dash) interactions of Furnstahl and Wallace. The lower panel curves are based on our DBHF interaction.

folding model for elastic proton scattering from ^{40}Ca at 200 MeV. The quality of the agreement is similar to that seen in Fig. 5. The solid curve on the lower panels uses the Furnstahl and Wallace elastic-scattering interaction in a folding model. In this case agreement is better for both the cross section and the analyzing power. If instead the Furnstahl and Wallace inelastic interaction is used, the cross section rises and the analyzing power moves toward negative values (long and short dash curves). Thus a large part of the difference between our DBHF model and the elastic-scattering data arises because our density-dependent interaction is calculated in infinite nuclear matter, which ignores any specific state dependence of the *G* matrix.

This raises the question of the degree to which the inelastic calculations we report are sensitive to this issue. We address this point by comparing two calculations for the excitation of the first 3^- state in ^{40}Ca (see upper panels of Fig. 7). Both calculations are based on Furnstahl and Wallace interactions. Pauli blocking and binding energy effects have been included [28]. The solid curve is their standard prescription with the elastic interaction used to produce the folding model distortions. The dot-dashed curve uses the same inelastic interaction for both the folding model distortions and the DWIA calculation of the transition. This change has the effect of again moving the cross section up and the analyzing power to more negative values, but the changes for inelastic scattering are more modest. Near the peak of the cross section, almost no difference exists.

For comparison, we show in the lower panels of Fig. 7 the same data for the 3^- transition in ^{40}Ca in comparison with the DBHF calculations from our model. All calculations overestimate the cross section. The DBHF model, if renormalized, gives the best representation of the diffractive shape of the angular distribution. Near the peak of the cross section, the prediction of the analyzing power is excellent in all cases. As the cross section declines, differences appear. The DBHF model presented here then falls below the measurements, much as the Furnstahl-Wallace model calculation does when the inelastic interaction is used to generate the folding model distortions. Thus the use of infinite nuclear matter to produce the density-dependent interaction will lead to discrepancies on the order of the differences seen in the upper panels of Fig. 7. This will need to be remembered in the interpretations to follow.

B. Results

We will now present a variety of results with the purpose of evaluating the quality of our description of the density-dependent effects. The goal of this section is to illustrate the DBHF calculations for a variety of transitions chosen to explore systematic trends that might affect the quality of the agreement with data. After reviewing elastic scattering, we will examine some of the strongest collective states. The form factors for these states are among the best known since the electron-scattering data is of especially high quality. These transitions tend to emphasize momentum transfers near 0.5–1.5 fm^{-1} since the total angular momentum transfer is usually $\Delta J = 2$ or 3. To check smaller and larger momentum transfers, we will then look at states with smaller and larger spins. Finally, the 2^+ excited states of ^{28}Si offer an opportunity to examine the DBHF model at different nuclear densities since there is a large variety of radial distributions for the transition form factors among these states [47].

To facilitate comparisons, in each of Figs. 8–12 the DBHF model results are represented by solid curves. The density dependence that arises only from the BHF mechanisms is shown by long dashed curves. The free interaction is shown for reference as short dashed curves. In each case the folding model distortions and the DWIA transition are calculated with the same interaction.

We start with some additional comments on elastic scattering. Figure 8 shows the folding model calculations for proton elastic scattering from ^{16}O and ^{28}Si at 200 MeV. The local nuclear matter density was derived from the longitudinal electron scattering form factor [61]. The data for ^{28}Si were taken in connection with an investigation of high-spin states in that nucleus [37]. The features here are similar to those described above for ^{40}Ca. The DBHF calculations in their present form overestimate the cross section and predict values for the analyzing power that are generally too negative. In the analyzing power, we see a progression from positive to negative values as the size of the density dependence increases through BHF to DBHF. Clearly the reduction of the density dependence present in the Furnstahl and Wallace calculations would be helpful here, as discussed previously.

Figure 9 shows data for three strong collective states along with the three sets of DWIA calculations. In all cases the peak of the cross section is overpredicted by about 50%. A number of factors have been included that reduce the calculated cross section, including relativistic kinematics for the

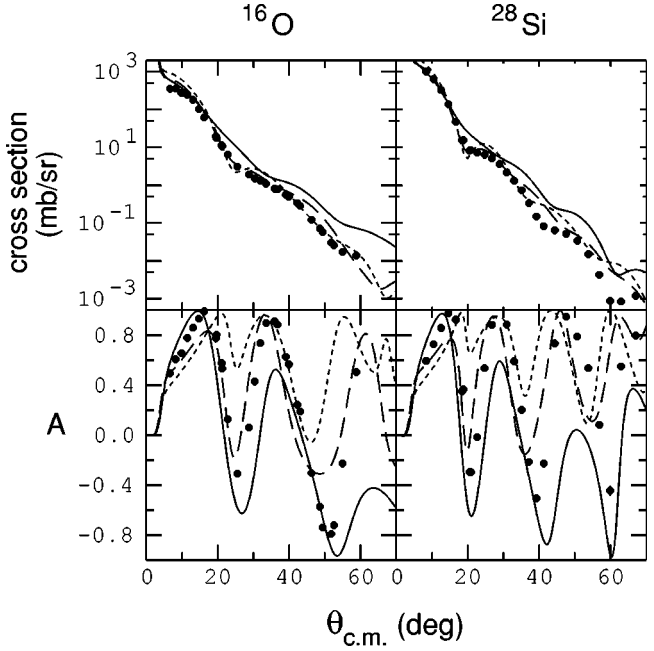

FIG. 8. Measurements of the cross section and analyzing power for ^{16}O and ^{28}Si at 200 MeV. The folding model calculations are based on the free (short dash), BHF (long dash), and DBHF (solid) forms of the effective interaction.

transformation from *t* matrix to the Yukawa expansion and the transformation of the interaction from *NN* to *N*-nucleus coordinates described by Eq. (14) of Love and Franey [44]. This overestimate has been an issue in other investigations, and has been handled in the empirical interaction of the Kelly group [46,47] by attenuating the free interaction by a factor of about 0.8. There the overestimate has been ascribed to an inadequacy in the local-density approximation. At lower bombarding energies such overestimates of the cross section in DWBA calculations have been attributed to distorted wave functions that are too large in the nuclear interior

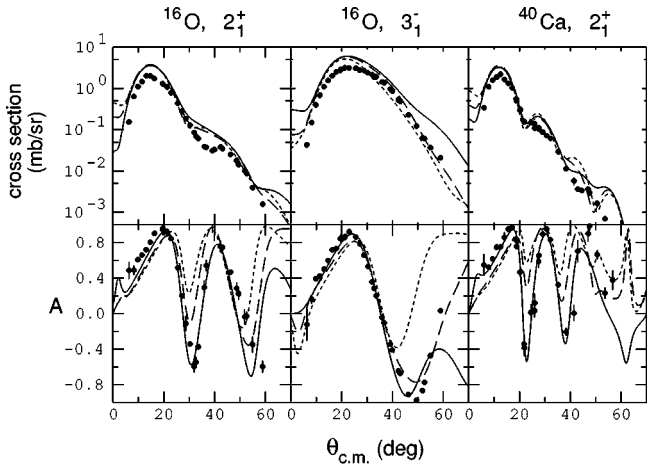

FIG. 9. Measurements of the cross section and analyzing power for the (p,p') reaction leading to the 2^+ and 3^- states in ^{16}O at 6.917 and 6.130 MeV, and the 2^+ state in ^{40}Ca at 3.904 MeV. The DWIA curves are based on the free (short dash), BHF (long dash), and DBHF (solid) interactions.

because they ignore the exchange nonlocalities described by Perey and Buck [70]. Inclusion of this correction (derived from the energy dependence of the strength of the central optical model potential) in fact increases the cross section at the peak and does not, at least its standard form, represent a helpful way to handle this issue. Generally, the shapes of the cross section angular distributions match the main features of the data. Except for the tendency of the DBHF calculation to remain too large at large scattering angles (see the 3^- state in ^{16}O), the quality of the agreement is not good enough in detail to make a comparative evaluation of the quality of the BHF and DBHF calculations. This large angle enhancement arises mainly from the density-dependent increase in the size of the spin-orbit interaction.

Of the three calculations shown, the best reproduction of the analyzing power is clearly with the DBHF predictions. The strong density dependence of the DBHF model raises the analyzing powers at angles forward of the cross section maximum and lowers it beyond, something that is needed to get a better representation of the data. Based on the agreement here to the analyzing power, a model that is consistent with the bulk properties of nuclear matter is also best for nucleon-induced inelastic scattering.

Near the peak of the cross section, the analyzing power, described by Eq. (21a) of Love and Franey [44], is dominated by the positive values of the interference between the real spin-orbit and imaginary central effective interactions. In the DBHF model the reduced effective nucleon mass [22] enhances the real spin-orbit interaction (see Fig. 4 of Ref. [27]), leading to more positive values of the analyzing power. This effect is much smaller at $q<1$ fm^{-1} for the BHF model (see Fig. 4 of Ref. [46]). Dramatic improvements are also present with the DBHF model for the diffractive oscillations in the analyzing power. This effect cannot be described with such a plane-wave argument. In contrast, the cross section, which in plane wave is the incoherent sum of the central and spin-orbit magnitudes, shows smaller effects near the peak because of the balance between decreasing central and increasing spin-orbit contributions.

For the weaker (p,p') transitions, agreement with the calculations is a bit more elusive. In Fig. 10, we again show the three types of calculations for the 0^+ state in ^{28}Si at 4.98 MeV and the 1^- state in ^{16}O at 7.117 MeV, both noncollective transitions of low spin. For the most part, the general features of the cross sections are reproduced. Again, the DBHF model provides a better description of the analyzing powers, but the differences between the BHF and DBHF results for the 0^+ state are mixed. These results are less supportive of the quality of the interaction at low momentum transfer than was noted for the large collective states in Fig. 9.

The higher spin states shown in Fig. 11 have simpler angular distributions. Here the quality of the reproduction is comparable to the strong collective states shown in Fig. 9. All of the analyzing powers show a falling angular distribution between 20° and 40° that is well reproduced and shows little sensitivity to density dependence. The overestimate of the cross section is still present. In all of the cases examined so far, the agreement with the data deteriorates at the larger

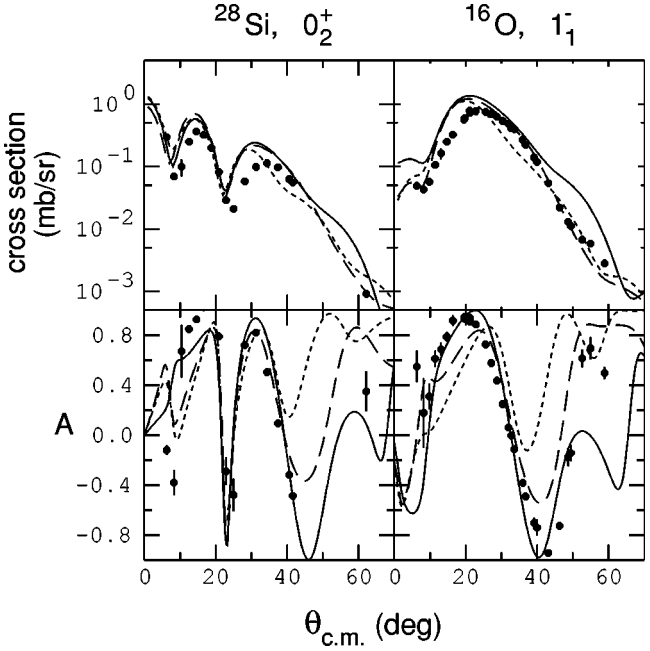

FIG. 10. Measurements of the cross section and analyzing power for the 0^+ state in ^{28}Si at 4.98 MeV and the 1^- state in ^{16}O at 7.117 MeV, along with calculations as described in Fig. 9.

angles, usually around 50°. Since the cross section at these larger angles is down at least an order of magnitude below its maximum, it is not clear that we can separate inadequacies of the interaction from inadequacies in the DWIA treatment.

Last, we examine whether the DBHF effects vary correctly with changing nuclear density. We will do so by examining states whose transition strengths occur at nuclear densities that are sufficiently different from each other to make a meaningful comparison. This opportunity is present for ^{28}Si where a series of 2^+ states shows the needed variety. In Fig. 12, the states considered in this analysis (cleanly resolved in the experiment) are shown from left to right in

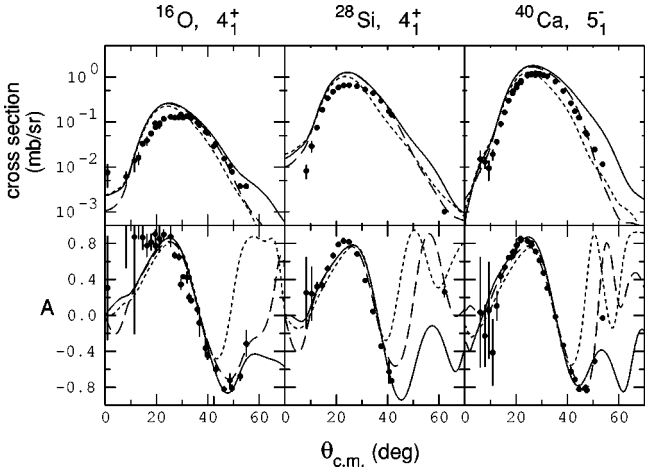

FIG. 11. Measurements of the cross section and analyzing power for the 4^+ state in ^{16}O at 10.356 MeV, the 4^+ state in ^{28}Si at 4.62 MeV, and the 5^- in ^{40}Ca at 4.492 MeV, along with calculations as described in Fig. 9.

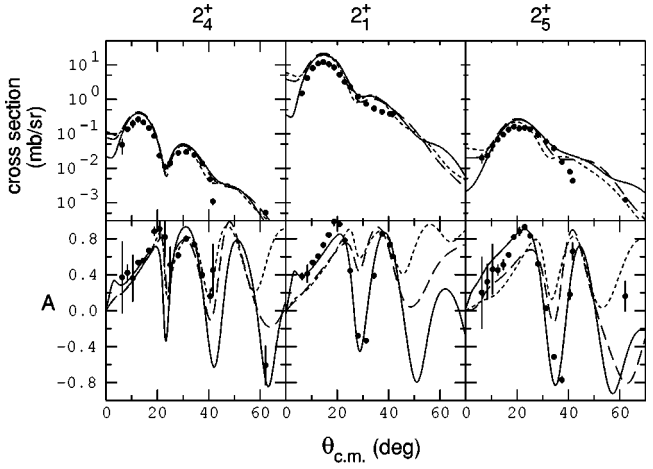

FIG. 12. Measurements of the cross section and analyzing power for three 2^+ states in ^{28}Si at 7.933, 1.779, and 8.259 MeV (in order of increasing nuclear density), along with calculations as described in Fig. 9.

order of decreasing reaction radius. This change is apparent from the expansion of the diffraction pattern as the reaction radius decreases. When the reaction radius is relatively large, then one would expect that most of the transition takes place in regions of the nucleus where the density is small and that changes to the effective *NN* interaction would be modest. This appears to be the case, as the size of the density-dependent modifications increases going from left to right in Fig. 12. This is true of both the cross section and the analyzing power. As the radius moves the transition to regions of higher nuclear density, the DBHF calculations do overall a better job of following the measurements. There are some problems describing the transition with the lowest density, as seen from the first state in Fig. 12, which may indicate that the density dependence is too strong at low density.

Overall, the DBHF interaction appears to provide a reasonable basis for density-dependent distortions and the effective interaction in the (p,p') transitions we considered here. However, there are systematic issues. In all cases, the cross section is overestimated. Detailed agreement with shape is often tricky if the data contains sharp diffractive oscillations. Even the use of form factors fit to (e,e') measurements does not constrain the cross section to tight agreement with (p,p') angular distributions. The DWIA together with the DBHF scheme appears to do best for angles near the maximum in the cross section. There the analyzing power almost always comes very close to the measurements. The analyzing power is also very sensitive to the choice of model (free, BHF, or DBHF) and the higher quality of agreement favors the DBHF model, even though the density dependence present in the folding model distortions remains too strong. This density dependence could, in principle, be reduced through a treatment of the *G* matrix for finite nuclear systems.

IV. CONCLUSIONS

The primary focus of this paper has been to explore a basis for inelastic scattering calculations with a medium-

modified effective *NN* interaction. To assess the quality of that basis, we have compared calculations to isoscalar, natural-parity transitions where medium effects from the established many-body models are known to be largest. We reported our predictions for several such states obtained in (p,p') inelastic scattering at energies near 200 MeV.

Our starting interaction is based on a relativistic OBE model with input parameters optimized to agree with the most modern sets of phase shift solutions to the *NN* scattering data base. We observed that it is important to start from an accurate two-body force. Medium effects are accounted for via a Dirac-Brueckner many-body approach. The proper handling of the nucleon in the medium through a correlated Dirac wave function provides a crucial saturation mechanism. Thus this framework describes realistically not only *NN* scattering data, but also the ground-state properties of nuclear matter through a self-consistent (that is, free of additional parameters) calculation.

We compared our DBHF predictions with those from the relativistic model of Furnstahl and Wallace and find similar quality of agreement for inelastic scattering. For elastic scattering, Furnstahl and Wallace achieve a better agreement with data. This arises from the fact that Furnstahl and Wallace treat nucleons as Dirac bound states in the nucleus, rather than infinite nuclear matter spinors.

Agreement of the DBHF model with inelastic scattering is satisfactory, although the quality of the predictions for the cross section deteriorates at the larger angles. At the same time, our DBHF model provides a very good description of the analyzing power, particularly in the angular region near the cross section peak. The analyzing power is also very sensitive to the model for the density dependence, and our results suggest that the density-dependent *NN* force given by the DBHF model is essentially correct.

Some systematic problems remain with the cross-section angular distributions, where the size is overestimated by about 50%. This problem persists regardless the particular effective interaction used, and may originate in the choice of the DWIA as a reaction mechanism.

In closing, we observe that a quantitative, relativistic two-body force combined with a Dirac approach to nuclear matter captures the main features of the (p,p') data considered here, particularly for the analyzing power. A similar framework has already proven successful in microscopic nuclear structure calculations [71]. Thus the scheme where a quantitative two-body force is applied self-consistently in the medium continues to provide a satisfactory picture of a wide range of nuclear processes. For future studies involving the spin dependence of the in-medium *NN* interaction, this model appears to be a satisfactory basis on which to proceed.

ACKNOWLEDGMENTS

We acknowledge the assistance of Malcolm Macfarlane with the transformation from *G* matrix to effective *NN* interaction. This paper was produced with financial assistance from the U.S. NSF under Grant No. NSF-PHY-9602872, a NATO travel Grant No. 900235, the University of Idaho Physics Department, and the University of Idaho Research Council.

APPENDIX A

In this appendix, we describe a transformation between the *S*-matrix or *t*- (*G*-) matrix representation of (in-medium) *NN* scattering and the expansion of the effective *NN* interaction in terms of Yukawa functions, as described by Love and Franey [44]. The five *NN* interaction amplitudes for the two isospin operators, **1** and $\tau_1\cdot\tau_2$, are separated by spin operator according to

$$t=t_0+t_\sigma\sigma_1\cdot\sigma_2+t_{LS}(\sigma_1+\sigma_2)\cdot n+t_{TD}S_{12}(\hat{q})+t_{TX}S_{12}(\hat{Q}) \tag{A1}$$

with $\hat{\mathbf{q}}=(\mathbf{k}'-\mathbf{k})/|\mathbf{k}'-\mathbf{k}|$, $\hat{\mathbf{n}}=(\mathbf{k}\times\mathbf{k}')/|\mathbf{k}\times\mathbf{k}'|$, and $\hat{\mathbf{Q}}=\hat{\mathbf{q}}\times\hat{\mathbf{n}}$. The five pieces in order are the central, spin-spin, spin-orbit, tensor direct, and tensor exchange. The direct part of each amplitude t_i is represented by the sum of 2–4 Yukawa functions. The exchange part is computed from the direct using the symmetries of *NN* scattering [44]. When combined with the direct for the free case, this gives a set of amplitudes that describe *NN* scattering measurements.

The Yukawa functions in coordinate space are [44]

$$t_C(r)=\sum_\alpha V_\alpha^C Y(r/R_\alpha),$$

where

$$Y(x)=e^{-x}/x, \tag{A2}$$

$$t_S(r)=\sum_\alpha V_\alpha^S Y(r/R_\alpha), \tag{A3}$$

$$t_T(r)=\sum_\alpha V_\alpha^T r^2 Y(r/R_\alpha), \tag{A4}$$

with the Fourier transforms

$$t_C(k)=4\pi\sum_\alpha \frac{V_\alpha^C R_\alpha^3}{1+(kR_\alpha)^2}, \tag{A5}$$

$$t_S(k)=8\pi\sum_\alpha \frac{V_\alpha^S kR_\alpha^5}{[1+(kR_\alpha)^2]^2}, \tag{A6}$$

$$t_T(k)=32\pi\sum_\alpha \frac{V_\alpha^T k^2 R_\alpha^7}{[1+(kR_\alpha)^2]^3}. \tag{A7}$$

The V_α^C, V_α^S, and V_α^T are the central, spin-orbit, and tensor Yukawa coefficients, and the R_α are their associated ranges. A single set of coefficients V_α can be used for either a coordinate- or momentum-space representation of *t*.

The *S*-matrix elements that describe (medium-modified) *NN* scattering may be obtained from the (complex) phase shifts according to

$$S_n=e^{\delta_n}, \tag{A8}$$

if the phase is uncoupled, or

$$S_n=\begin{pmatrix} e^{2i\delta_l}\cos 2\epsilon & ie^{i(\delta_l+\delta_{l'})}\sin 2\epsilon \\ ie^{i(\delta_l+\delta_{l'})}\sin 2\epsilon & e^{2i\delta_{l'}}\cos 2\epsilon \end{pmatrix}, \tag{A9}$$

if the phase shifts are coupled. Here the quantum numbers n include the total angular momentum J, the total spin S, the total isospin T, and the orbital angular momenta l and l'. The S-matrix elements are related to the t-matrix elements through

$$S^{JST}_{l'l}(p)=\delta_{l'l}-i\kappa t^{JST}_{l'l}(p). \tag{A10}$$

The coefficient $\kappa=2\pi\mu p$ where μ is the reduced mass in the *NN* system and p is the *NN* center-of-mass momentum. It is the values of $t^{JST}_{l'l}(p)$ that are available from the G-matrix calculation.

To adequately represent the pion tail, we calculate $t^{JST}_{l'l}(p)$ matrix elements through $J=15$. A satisfactory Yukawa expansion need contain no more than the 44 coefficients used by Franey and Love [53] in their 210-MeV interaction. With $t^{JST}_{l'l}(p)$ matrix elements outnumbering Yukawa coefficients, a least-squares minimization was employed to choose the best coefficient values. The transformation matrix **M** connects these two spaces through **G**=**MV** where **G** and **V** are vectors containing, respectively, the $t^{JST}_{l'l}(p)$ matrix elements and the V_α Yukawa coefficients. Since **M** is linear, the minimization process may be accomplished in one step. Defining

$$\mathcal{G}_j=\sum_i G_i M_{ij}, \tag{A11}$$

$$\mathcal{M}_{jk}=\sum_i M_{ik}M_{ij}, \tag{A12}$$

the solution becomes

$$V_k=\sum_j \mathcal{M}^{-1}_{jk}\mathcal{G}_j. \tag{A13}$$

The ranges are fixed in advance of the fit at the values used by Franey and Love [53].

The closed-form expression for the elements of the transform matrix **M** is

$$\begin{aligned} t^{JST}_{l'l}=\frac{1}{2p^2}\Bigg(& \delta_{l'l}g^{ST}_C(l,p)-6\,\delta_{l'l}\delta_{S1}(-)^{l+J}\begin{Bmatrix} l & J & 1\\ 1 & 1 & l\end{Bmatrix}\Bigg[\sum_\lambda (2\lambda+1)\langle\lambda 100|l0\rangle^2\begin{Bmatrix} l & l & 1\\ 1 & 1 & \lambda\end{Bmatrix}g^T_S(\lambda,p)\Bigg] \\ & -(-)^{(l'-l)/2}2\sqrt{30}\delta_{S1}(-)^{l'+J+3}\begin{Bmatrix} l' & J & 1\\ 1 & 2 & l\end{Bmatrix}\Bigg[\sqrt{2l'+1}\langle l'200|l0\rangle\frac{1}{p^2}[g^T_T(l,p)+g^T_T(l',p)]+\sqrt{30}\sum_\lambda (2\lambda+1) \\ & \times\langle\lambda 100|l'0\rangle\langle\lambda 100|l0\rangle\begin{Bmatrix} l' & l & 2\\ 1 & 1 & \lambda\end{Bmatrix}\frac{1}{p^2}g^T_T(\lambda,p)\Bigg]\Bigg). \end{aligned} \tag{A14}$$

The sums on λ run from the maximum of $l-1$ or $l'-1$ to the minimum of $l+1$ or $l'+1$. The Yukawa coefficients are contained in the expressions for the g functions as

$$g^{ST}_C(l,p)=\sum_\alpha V^C_\alpha R_\alpha Q_\alpha(y_\alpha), \tag{A15}$$

$$g^T_S(l,p)=\sum_\alpha V^S_\alpha R_\alpha Q'_\alpha(y_\alpha), \tag{A16}$$

$$g^T_T(l,p)=\sum_\alpha V^T_\alpha R_\alpha Q''_\alpha(y_\alpha), \tag{A17}$$

where the Q_α are Legendre functions of the second kind and the derivatives are with respect to y_α where

$$y_\alpha=1+\frac{1}{2p^2R^2_\alpha}. \tag{A18}$$

The details of this transform were provided by Malcolm Macfarlane, who derived them as part of a study of the off-shell unitarity of the effective *NN* interaction [72].

APPENDIX B

For proton inelastic scattering to a specific state of the target nucleus, the laboratory energy as a function of angle for the scattered proton will differ significantly from the values for free *NN* scattering. Thus we must adopt a model for choosing the momentum transfer q and crossed momentum transfer Q that will be used to evaluate the direct and exchange pieces, respectively, of the effective interaction. For the calculations reported in this paper, the model described in this appendix replaces the standard choice in the program LEA [45] of fixing Q at all angles to be the value associated with 0° scattering.

In the center-of-mass frame, a projectile with momentum **k** scatters at an angle θ, leaving with the new momentum **k**′. For reactions with a nonvanishing Q value, the magnitudes of these two momenta are not equal, $k'\neq k$. The momentum transfer for the direct amplitude is taken to be **q**=**k**′−**k**. The

vector **q** lies at an angle φ, $0 \leqslant \varphi \leqslant \pi/2$, with respect to the beam axis. Using this choice for **q** to evaluate the direct amplitude is consistent with the assumption that the projectile makes an on-shell scattering from a nucleon in the target that is in motion prior to the collision. Binding-energy effects are neglected.

The model for the crossed momentum transfer Q begins by choosing the momentum $\mathbf{k}_t$ for the struck nucleon to have the smallest possible value in the target frame of reference consistent with on-shell scattering. This imposes two conditions that are determined nonrelativistically for a target of mass A. First, the projection of $\mathbf{k}_t$ on the momentum transfer axis must be $q/2$ to maintain on-shell kinematics. Second, the projection of $\mathbf{k}_t$ perpendicular to the momentum transfer axis in the scattering plane must be the same as the projection of the struck nucleon's share of the target momentum, $-\mathbf{k}/A$, onto the same direction. This minimizes the momentum of the struck nucleon in the target frame of reference. With $\mathbf{k}_t$ thus constrained, $\mathbf{Q}=\mathbf{k}'-\mathbf{k}_t$. The magnitude of Q used to evaluate the exchange amplitude is most easily expressed in terms of its components, Q_x and Q_y with $Q^2 = Q_x^2 + Q_y^2$, as

$$Q_x = k' \cos\theta + \frac{k}{A} + h \cos\varphi, \tag{B1}$$

and

$$Q_y = k' \sin\theta - h \sin\varphi, \tag{B2}$$

where

$$h = \frac{q}{2} - \frac{k}{A}\cos\varphi. \tag{B3}$$

Relaxing the second condition to include larger values of the struck nucleon momentum in the target frame, and with a variety of possible directions, results in values of Q that can be either smaller or larger than the one described above. Thus this model for Q does not depend strongly on the momentum of the struck nucleon being very close to the limiting case of minimal size in the target frame.

Exchange amplitudes calculated using this model were compared with the exact finite-range amplitudes from DWBA86 [62] in the preparation of a study of the strong 6^- transitions in ^{28}Si [37]. The results were clearly superior to those calculated using the fixed value of Q.

[1] K. A. Brueckner, C. A. Levinson, and H. M. Mahmoud, Phys. Rev. **95**, 217 (1954).
[2] H. A. Bethe, Phys. Rev. **103**, 1353 (1956).
[3] J. Goldstone, Proc. R. Soc. London, Ser. A **239**, 267 (1957).
[4] H. A. Bethe, Annu. Rev. Nucl. Sci. **21**, 93 (1971).
[5] M. I. Haftel and F. Tabakin, Nucl. Phys. **A158**, 1 (1970).
[6] D. W. L. Sprung, Adv. Nucl. Phys. **5**, 225 (1972).
[7] F. A. Brieva and J. R. Rook, Nucl. Phys. **A291**, 299 (1977); **A291**, 317 (1977); **A297**, 206 (1978).
[8] L. Ray and G. W. Hoffmann, Phys. Rev. C **31**, 538 (1985).
[9] S. Karatiglidis, P. J. Dortmans, K. Amos, and R. de Swiniarski, Phys. Rev. C **53**, 838 (1996).
[10] P. J. Dortmans, K. Amos, and S. Karatiglidis, J. Phys. G **23**, 183 (1997).
[11] M. A. Suhail, S. M. Saliem, and W. Haider, J. Phys. G **23**, 365 (1997).
[12] S. P. Weppner, Ch. Elster, and D. Hüber, Phys. Rev. C **57**, 1378 (1998).
[13] E. Bauge, J. P. Delaroche, and M. Girod, Phys. Rev. C **58**, 1118 (1998).
[14] G. Q. Li, R. Machleidt, R. Fritz, H. Müther, and Y. Z. Zhou, Phys. Rev. C **48**, 2443 (1993).
[15] H. V. von Geramb, *The Interaction Between Medium Energy Nucleons in Nuclei—1982*, AIP Conf. Proc. No. 97 (AIP, New York, 1983), p. 44.
[16] L. Rikus, K. Nakano, and H. V. von Geramb, Nucl. Phys. **A414**, 413 (1984).
[17] J. J. Kelly *et al.*, Phys. Rev. C **39**, 1222 (1989); see also references in [46].
[18] James J. Kelly, Phys. Rev. C **39**, 2120 (1989).
[19] K. Nakayama and W. G. Love, Phys. Rev. C **38**, 51 (1988).
[20] L. Ray, Phys. Rev. C **41**, 2816 (1990).
[21] S. Karatiglidis, P. J. Dortmans, K. Amos, and R. de Swiniarski, Phys. Rev. C **52**, 861 (1995).
[22] R. Machleidt, Adv. Nucl. Phys. **19**, 189 (1989).
[23] M. R. Anastasio, L. S. Celenza, W. S. Pong, and C. M. Shakin, Phys. Rep. **100**, 327 (1983).
[24] R. Brockmann and R. Machleidt, Phys. Lett. **149B**, 283 (1984); Phys. Rev. C **42**, 1965 (1990).
[25] C. J. Horowitz and B. D. Serot, Phys. Lett. **137B**, 287 (1984); Nucl. Phys. **A464**, 613 (1987).
[26] B. ter Haar and R. Malfliet, Phys. Rep. **149**, 207 (1987).
[27] R. J. Furnstahl and S. J. Wallace, Phys. Rev. C **47**, 2812 (1993).
[28] J. J. Kelly and S. J. Wallace, Phys. Rev. C **49**, 1315 (1994).
[29] L. Kurth, B. C. Clark, E. D. Cooper, S. Hama, S. Shim, R. L. Mercer, L. Ray, and G. W. Hoffmann, Phys. Rev. C **49**, 2086 (1994).
[30] L. B. Rees, J. M. Moss, T. A. Carey, K. W. Jones, J. B. McClelland, N. Tanaka, A. D. Bacher, and H. Esbensen, Phys. Rev. C **34**, 627 (1986).
[31] C. Chan *et al.*, Nucl. Phys. **A510**, 713 (1990).
[32] X. Y. Chen *et al.*, Phys. Rev. C **47**, 2159 (1993).
[33] T. N. Taddeucci *et al.*, Phys. Rev. Lett. **73**, 3516 (1994).
[34] S. W. Wissink, in *Spin and Isospin in Nuclear Interactions*, edited by S. W. Wissink *et al.* (Plenum, New York, 1991), p. 253.
[35] E. J. Stephenson and J. A. Tostevin, in *Spin and Isospin in Nuclear Interactions* (Ref. [34]), p. 281.
[36] H. Baghaei *et al.*, Phys. Rev. Lett. **69**, 2054 (1992).

[37] E. J. Stephenson, J. Liu, A. D. Bacher, S. M. Bowyer, S. Chang, C. Olmer, S. P. Wells, and S. W. Wissink, Phys. Rev. Lett. **78**, 1636 (1997).
[38] A. De Pace, Phys. Rev. Lett. **75**, 29 (1995).
[39] C. J. Horowitz and D. P. Murdock, Phys. Rev. C **37**, 2032 (1988).
[40] H. Toki and I. Tanihata, Phys. Rev. C **59**, 1196 (1999).
[41] G. E. Brown, M. Buballa, Zi Bang Li, and J. Wambach, Nucl. Phys. **A593**, 295 (1995).
[42] G. E. Brown and M. Rho, Phys. Rev. Lett. **66**, 2720 (1991); Phys. Rep. **269**, 334 (1996).
[43] T. Hatsuda and T. Kunihiro, Phys. Rep. **247**, 221 (1994), and references therein.
[44] W. G. Love and M. A. Franey, Phys. Rev. C **24**, 1073 (1981).
[45] James J. Kelly, Program Manual for LEA, 1995.
[46] H. Seifert *et al.*, Phys. Rev. C **47**, 1615 (1993).
[47] Q. Chen, J. J. Kelly, P. P. Singh, M. C. Radhakrishna, W. P. Jones, and H. Nann, Phys. Rev. C **41**, 2514 (1990).
[48] Jian Liu, E. J. Stephenson, A. D. Bacher, S. M. Bowyer, S. Chang, C. Olmer, S. P. Wells, S. W. Wissink, and J. Lisantti, Phys. Rev. C **53**, 1711 (1996).
[49] R. H. Thompson, Phys. Rev. D **1**, 110 (1970).
[50] R. Machleidt, *One-Boson Exchange Potentials and Nucleon-Nucleon Scattering*, Comp. Nucl. Phys. 2—Nucl. Reactions, edited by K. Langanke, J. A. Maruhu, and S. E. Koonin (Springer, New York, 1993), p. 1.
[51] V. G. J. Stoks *et al.*, Phys. Rev. C **49**, 2950 (1994).
[52] R. Machleidt, F. Sammarruca, and Y. Song, Phys. Rev. C **53**, 1483 (1996); (unpublished).
[53] M. A. Franey and W. G. Love, Phys. Rev. C **31**, 488 (1985).
[54] M. Lacombe *et al.*, Phys. Rev. C **21**, 861 (1980).
[55] R. V. Reid, Jr., Ann. Phys. (N.Y.) **50**, 411 (1968).
[56] F. Sammarruca and E. J. Stephenson, Phys. Rev. C **58**, 307 (1998).
[57] L. G. Arnold, B. C. Clark, and R. L. Mercer, Phys. Rev. C **19**, 917 (1979).
[58] T. Cheon, K. Takayanagi, and K. Yazaki, Nucl. Phys. **A437**, 301 (1985); **A445**, 227 (1985).
[59] T. Cheon and K. Takayanagi, Nucl. Phys. **A455**, 653 (1986).
[60] A. K. Kerman, H. McManus, and R. M. Thaler, Ann. Phys. (N.Y.) **8**, 551 (1959).
[61] H. de Vries, C. W. De Jager, and C. De Vries, At. Data Nucl. Data Tables **36**, 495 (1987).
[62] R. Schaeffer and J. Raynal, program DWBA70; S. Austin, W. G. Love, J. R. Comfort, and C. Olmer, extended version DWBA86 (unpublished).
[63] J. Raynal, Nucl. Phys. **97**, 572 (1967).
[64] Program OXBASH, B. A. Brown, A. Etchegoyen, and W. D. M. Rae, MSU-NSCL Report No. 54.
[65] B. A. Brown and B. H. Wildenthal, Annu. Rev. Nucl. Part. Sci. **38**, 29 (1988).
[66] C. A. Olmer *et al.*, Phys. Rev. C **29**, 861 (1984).
[67] H. O. Meyer *et al.*, Phys. Rev. C **23**, 616 (1981).
[68] P. Schwandt, H. O. Meyer, W. W. Jacobs, A. D. Bacher, S. E. Vigdor, M. D. Kaitchuck, and T. R. Donoghue, Phys. Rev. C **26**, 55 (1982).
[69] J. A. Tjon and S. J. Wallace, Phys. Rev. C **35**, 280 (1987); **36**, 1085 (1987).
[70] F. Perey and B. Buck, Nucl. Phys. **32**, 353 (1962).
[71] M. F. Jiang *et al.*, Phys. Rev. C **46**, 910 (1992).
[72] M. H. Macfarlane and Edward F. Redish, Phys. Rev. C **37**, 2245 (1988).